nature photonics

REVIEW ARTICLE

PUBLISHED ONLINE: 30 JANUARY 2014 | DOI: 10.1038/NPHOTON.2013.238

Plasmon-induced hot-electron generation at nanoparticle/metal-oxide interfaces for photovoltaic and photocatalytic devices

César Clavero

Finding higher efficiency schemes for electron–hole separation is of paramount importance for realizing more efficient conversion of solar energy in photovoltaic and photocatalytic devices. Plasmonic energy conversion has been proposed as a promising alternative to conventional electron–hole separation in semiconductor devices. This emerging method is based on the generation of hot electrons in plasmonic nanostructures through electromagnetic decay of surface plasmons. Here, the fundamentals of hot-electron generation, injection and regeneration are reviewed, with special attention paid to recent progress towards photovoltaic devices. This new energy-conversion method potentially offers high conversion efficiencies, while keeping fabrication costs low. However, several considerations regarding the materials, architectures and fabrication methods used need to be carefully evaluated to advance this field.

The outstanding light-trapping and electromagnetic-field-concentrating properties of surface plasmons open up a wide range of applications in the field of plasmonics[1]. Localized surface plasmon resonance (LSPR) can occur in properly designed nanostructures in which confined free electrons oscillate with the same frequency as the incident radiation and eventually enter resonance, giving rise to intense, highly localized electromagnetic fields. Consequently, such nanostructures have been proposed as efficient light-trapping components that can be integrated in photovoltaic cells to increase the efficiency of conventional architectures considerably[2,3]. However, recent investigations have shown that plasmonic nanostructures can also directly convert the collected light into electrical energy by generating hot electrons[4–13]. After light absorption in the nanostructures and LSPR excitation, plasmons can decay, transferring the accumulated energy to electrons in the conduction band of the material. This process produces highly energetic electrons, also known as 'hot electrons', which can escape from the plasmonic nanostructures and be collected by, for example, putting the plasmonic nanostructures in contact with a semiconductor, thereby forming a metal–semiconductor Schottky junction[6]. This new scheme for solar energy conversion opens up a way to realize photovoltaic and photocatalytic devices whose performances may rival, or even exceed, those of conventional devices. However, some difficulties and limitations inherent to the nature of this energy conversion process and to the properties of the materials employed need to be addressed in order to achieve larger efficiencies while keeping fabrication costs low.

Plasmonic energy conversion

Plasmonic hot-electron generation. Electrons not in thermal equilibrium with the atoms in a material are frequently referred to as hot electrons. The term hot electrons refers to electrons whose distributions can be fundamentally described by the Fermi function, but with an elevated effective temperature[14]. When a material is illuminated with highly energetic photons (for example, ultraviolet radiation), hot electrons are generated and emitted from the material via the photoelectric effect[15]. Electrons whose energies exceed the work function of the material are emitted, producing a photocurrent. However, as the solar spectrum is mostly composed of less energetic visible and near-infrared photons, the use of this effect is impractical for photovoltaic devices. Hot electrons can also be generated by exothermic chemical processes[16,17], such as those that occur in dye-sensitized solar cells[18]. In these cells, a dye molecule anchored to a semiconductor absorbs incoming light and transfers energetic charge carriers to the semiconductor[19].

A major breakthrough in this field was the recent discovery of hot-electron generation in plasmonic nanostructures. Following light absorption and LSPR excitation in these nanostructures, electromagnetic decay takes place on a femtosecond timescale, either radiatively through re-emitted photons[20] (Fig. 1a, left) or non-radiatively by transferring the energy to hot electrons[12,21–23] (Fig. 1a, right). In the non-radiative process, surface plasmons first decay into single-electron excited states. This might be followed by photoemission if the electron energy exceeds the work function of the material[24]. Two-photon processes have also been described[23]. Non-radiative decay in noble-metal nanostructures can take place through intraband excitations within the conduction band or through interband excitations caused by transitions between other bands (for example, *d* bands) and the conduction band. However, the *d* band energy levels respectively lie 2.4 eV and 4 eV below the Fermi energy levels for Au and Ag, making interband excitations considerably more unlikely than intraband excitations[25,26]. The remaining photoexcited electrons relax through electron–electron and electron–phonon collisions, and are ultimately converted into heat[24].

Figure 1b depicts the parabolic density of states (DOS) in the conduction band of a plasmonic nanostructure with a Fermi energy $E_{F,M}$ as a function of energy. After non-radiative surface plasmon decay, electrons from occupied energy levels are excited above the Fermi energy. For example, surface plasmons in Au and Ag noble-metal nanostructures can transfer energies between approximately 1 eV and 4 eV to hot electrons; this energy depends

Plasma Applications Group, Environmental Energy Technologies Division, Lawrence Berkeley National Laboratory, 1 Cyclotron Road, Berkeley, California 94720, USA. e-mail: cclavero@lbl.gov

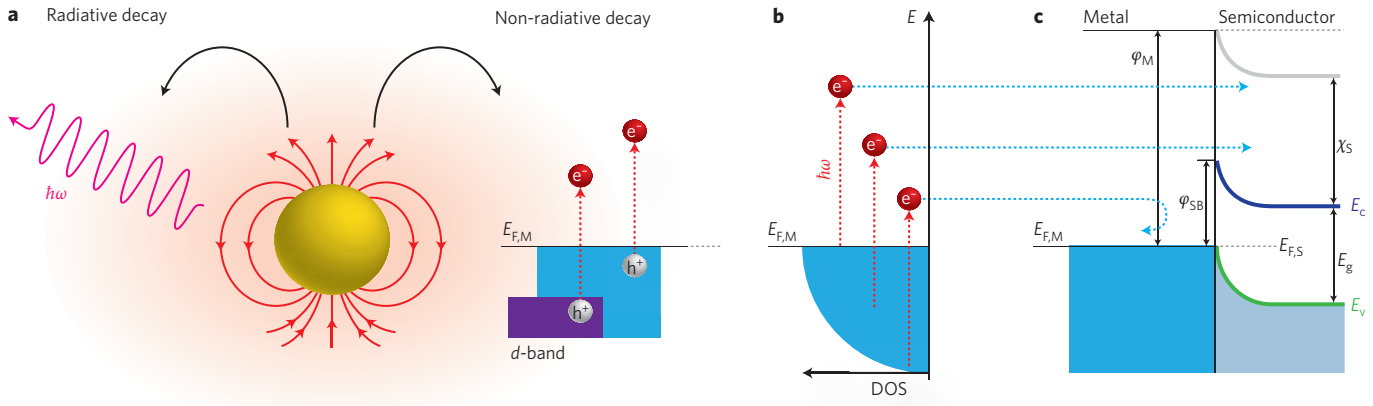

Figure 1 | Surface-plasmon decay, hot-electron generation and injection. a, Localized surface plasmons can decay radiatively via re-emitted photons or non-radiatively via excitation of hot electrons. In noble-metal nanostructures, non-radiative decay can occur through intraband excitations within the conduction band or through interband excitations resulting from transitions between other bands (for example, *d* bands) and the conduction band. **b**, Plasmonic energy conversion: electrons from occupied energy levels are excited above the Fermi energy. **c**, Hot electrons can be injected into a semiconductor by forming a Schottky barrier with the plasmonic nanostructure. Hot electrons with energies high enough to overcome the Schottky barrier $\varphi_{SB} = \varphi_M - \chi_S$ are injected into the conduction band E_c of the neighbouring semiconductor, where φ_M is the work function of the metal and χ_S is the electron affinity of the semiconductor.

on the carrier concentration and the size and shape of the nanostructures[9,20,27]. An efficient mechanism for capturing such hot electrons is to form a Schottky barrier with an appropriate semiconductor. Figure 1c shows a Schottky barrier between a plasmonic nanostructure and an n-type semiconductor, such as TiO_2. TiO_2 is a good electron-accepting metal oxide because of the high DOS in its conduction band; it thus permits fast electron injection. Hot electrons with energies higher than the Schottky barrier energy φ_{SB} can be injected into the semiconductor with an emission efficiency dependent on their energy[25]. In addition, tunnelling across the barrier can take place with a much lower probability[28]. The energy needed for hot electrons to overcome the energy barrier in this system is considerably smaller than the bandgap of the semiconductor E_g (refs 7,28). After injection of hot electrons into the neighbouring semiconductor, the plasmonic nanostructures are left positively charged because of electronic depletion. An electron-donor solution or a hole-transporting material (HTM) is required to be in contact with the nanostructures to transport the generated holes to the counter electrode, keeping the charge balance and sustaining an electric current.

As this Review will show, plasmonic devices are not affected by the thermodynamic factors that limit the efficiencies of conventional semiconductor-based devices, and they thus open a new horizon of possibilities in the field of solar energy conversion. The size, shape and composition of the plasmonic nanostructures can be adapted to obtain broad absorption across the whole solar spectrum. The high absorption cross-section of plasmonic nanostructures allows the thickness of the active zone to be reduced while maintaining a high light-trapping efficiency. In addition, recent studies have shown that their efficiency rises slightly with increasing temperature because of a higher probability of hot-electron injection[29].

First steps towards plasmonic energy conversion. Early studies published in 1996[4] showed hints of surface-plasmon-induced charge separation in noble-metal nanoparticles in contact with TiO_2. Zhao *et al.*[4] were the first to report an anodic photocurrent generated by visible-light illumination of a TiO_2 electrode with a TiO_2 overlayer containing gold or silver nanoparticles. This was a striking result because the wide bandgap (3.3 eV) of TiO_2 means that conventional TiO_2 electrodes generate photocurrents only when illuminated with ultraviolet light. The origin of these photocurrents was unclear at the time; Zhao *et al.* suggested the excitation of LSPR in the nanoparticles as a possible mechanism. This research field remained dormant for some years until 2003, when multicolour photochromism (that is, a reversible change in colour on illumination) in Ag nanoparticles dispersed in TiO_2 was reported[30]. This phenomenon was ascribed to LSPR-induced charge separation and oxidation of the Ag nanoparticles[30,31] (Fig. 2a). The inverse process, namely reversible injection of electrons from TiO_2 into Ag in core–shell Ag–TiO_2 nanoparticles, was also demonstrated by Hirakawa and Kamat[32].

Shortly after, several studies[5,6,33,34] demonstrated the three steps required to generate a photoinduced closed-circuit current — hot-electron generation, injection and regeneration. Systems consisting of Au or Ag nanoparticles absorbed onto nanoporous TiO_2 (which, in some cases, was in contact with an electron-donor solution) were investigated (Fig. 2b). Tian and Tatsuma[5,6] observed hot-electron injection into the TiO_2 matrix on excitation of LSPR in the nanoparticles by visible light illumination. Subsequently, compensative electrons from a donor solution in contact with the plasmonic nanoparticles were injected into the nanoparticles, balancing their electronic deficit and ultimately creating an electric circuit. The measured action spectra, which show the incident photon-to-electron conversion efficiency (IPCE) as a function of wavelength, exactly reproduced the extinction spectra of the Au nanoparticles, clearly demonstrating that LSPR plays a key role in promoting hot-electron generation (Fig. 2b).

Following these pioneering studies, very many studies have investigated plasmonic hot-electron generation with application to both photovoltaic and catalytic devices. Most of these studies investigated Au or Ag nanoparticles in contact with TiO_2[33–45] (Fig. 2c), but more recently multiple combinations of materials and architectures have been proposed. Some examples are multilayer assemblies of Au nanoparticles and TiO_2 nanosheets[46], Pt nanoparticles on TiO_2 thin films[47], Ag-decorated TiO_2 nanotube arrays[48,49] (Fig. 2d), ZnO nanorods decorated with Au nanoparticles[50,51], hierarchical Au–ZnO flower-rod heterostructures[52] (Fig. 2e), Au nanoparticles in contact with CeO_2[53,54], Au nanoprisms on WO_3[55], AgBr decorated with Ag nanoparticles and dispersed in Al_2O_3[56], Ag–AgI supported on mesoporous alumina[57], AgCl particles decorated with Ag nanoparticles[58], core–shell SiO_2–TiO_2 nanoparticles decorated with Au nanoparticles[59], M–TiO_2 core–shell nanocomposites (where M = Au, Pd, Pt)[60,61] (Fig. 2f), Au nanorods on Si[7] and Au–alumina–Au multilayers[8].

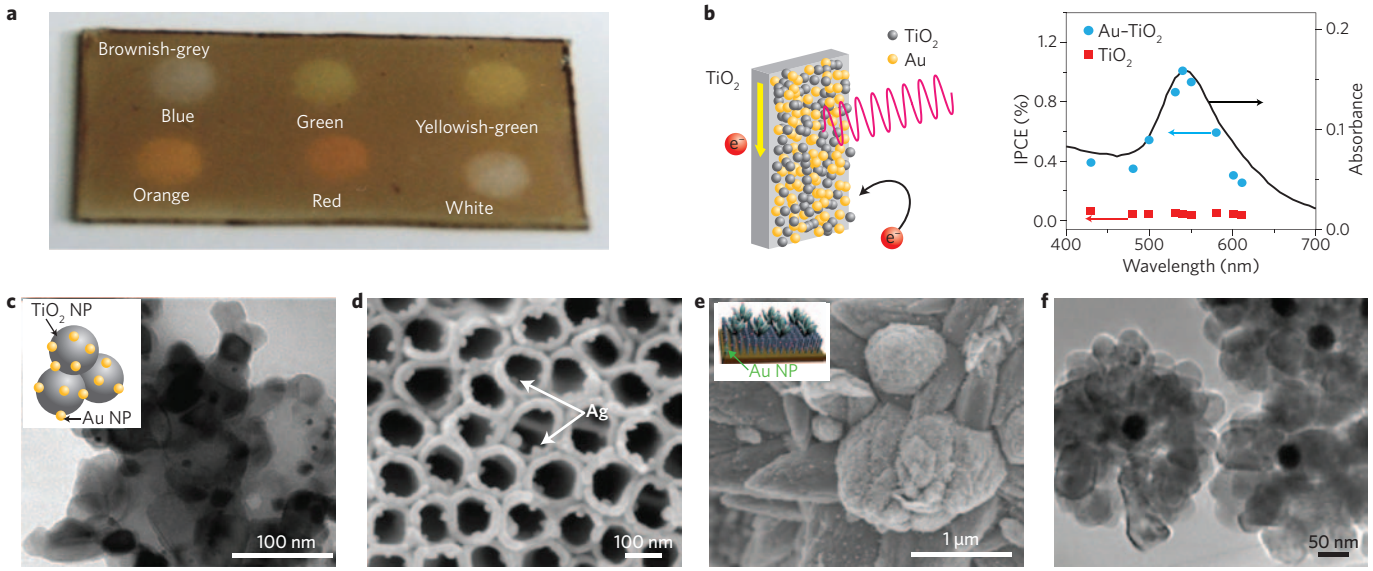

Figure 2 | Hot-electron generation by plasmonic nanostructures. a, Photochromism in Ag nanoparticles as a result of hot-electron generation[30]. **b**, Sketch of the system proposed by Zhao *et al.*[4] consisting of Au nanoparticles deposited on nanoporous TiO_2 (left). Tian *et al.*[5,6] used a similar system, but added an electron donor solution. The action spectra, that is, incident photon-to-electron conversion efficiency (IPCE), and extinction spectra share the same spectral shape. **c**, Transmission electron micrograph for Au-decorated TiO_2 nanoparticles[38]. **d**, Scanning electron micrograph of Ag in TiO_2 nanotubes[48]. **e**, Scanning electron micrograph of Au nanoparticles on ZnO flower-rod heterostructure[52]. **f**, Transmission electron micrographs of Au–TiO_2 core–shell nanoparticles[60]. Figure reproduced with permission from: **a**, ref. 30, © 2002 NPG; **b**, ref. 5, © RSC 2004; **c**, ref. 38, © 2011 ACS; **d**, ref. 48, © Springer 2012; **e**, ref. 52, © Springer 2013; **f**, ref. 60, © 2011 ACS.

Timescales of hot-electron generation, injection and regeneration. Fast-electron injection in the neighbouring semiconductor before carrier recombination is a key factor for increasing the efficiency of the energy conversion process. Several studies have focused on the timescales of the hot-electron generation, injection and regeneration mechanisms. They exploit the increased visible and infrared absorbance of TiO_2 when electrons are injected into the conduction band[6,62–64]. Furube and Du's group[11,62,65] have used ultrafast visible-pump/infrared-probe femtosecond transient absorption spectroscopy to characterize the charge transfer kinetics. Laser pulses (duration, 150 fs; wavelength, 550 nm) were used to excite LSPR in Au nanoparticles deposited on TiO_2 (Fig. 3a), while the transient absorption of TiO_2 at 3,500 nm was simultaneously monitored. The group found that hot-electron generation and injection completed within 50 fs. Because relaxation of electrons with a non-Fermi distribution in Au nanoparticles was found to occur through electron–electron (<100 fs), electron–phonon (1–10 ps) and phonon–phonon (~100 ps) interactions, the researchers concluded that electron injection occurs before or during thermalization as a result of electron–electron interaction[11,62,66]. Interestingly, comparison with ruthenium N3 dye on TiO_2, which is known to have a carrier injection efficiency of almost 100%, allowed them to determine that the injection efficiency was around 40% for Au–TiO_2 under 550-nm excitation. The injected hot electrons decay back to the nanoparticles after 1.5 ns when no donor solution is in contact with the Au nanoparticles, whereas carrier regeneration takes place when a donor solution is used. Tian *et al.*[63,64] investigated the timescale of the charge regeneration process when different electron-donor layers were in contact with the Au nanoparticles. They used $[Fe(CN)_6]^{4-}$, Fe^{2+}, ferrocenecarboxylic acid[63] and polyethylene oxide filled with TiO_2 nanoparticles containing optimized redox couples of I^-/I_3^- (ref. 64). The oxidized Au nanoparticles were shown to be totally regenerated in less than 20 ns in the presence of I^-, making this the fastest process. To further enhance the energy conversion efficiency of this process, it is critical to achieve faster hot-electron injection before energy loss occurs through electron–electron collisions and faster carrier regeneration by using optimized donor solutions or HTMs.

Effects of size and shape of plasmonic nanostructures. The size and shape of active plasmonic nanostructures are among the most important parameters for LSPR excitation and hot-electron generation. They affect not only the wavelength at which LSPR takes place, but also the efficiency of the charge separation process. As mentioned above, surface plasmons decay by either radiative emission of photons (the dominant process in large Au and Ag (20–40 nm) nanostructures[67]) or through non-radiative excitation of hot electrons (the dominant process for smaller nanostructures[9]). The nanostructure size at which radiative decay starts becoming the predominant process strongly depends on the optical characteristics of the material. Langhammer *et al.*[68] investigated this dependence in lithography-patterned Ag, Pt and Pd nanodisks with sizes ranging from 38 nm to 530 nm. Interestingly, non-radiative decay was found to be the dominant process for Pd and Pt nanodisks for all the investigated sizes, whereas it disappeared for Ag nanodisks larger than 110 nm. Yu *et al.*[34] observed larger photocurrents for 15-nm-diameter nanoparticles than in nanoparticles with larger diameters because of more efficient decay of surface plasmons into hot electrons in the 15-nm-diameter nanoparticles. In addition, spherical nanoparticles exhibit a single plasmon resonance peak, whereas structures such as nanorods exhibit two characteristic peaks that correspond to longitudinal and transverse modes. This phenomenon has been investigated in periodically distributed Au rods nanopatterned on TiO_2 single-crystal substrates[10,29] (Fig. 3b) and in nanorod-based plasmonic systems[13]. Double-peaked extinction spectra allow the optical absorption range to be extended, which is typically in the visible range for Au nanostructures, to the near-infrared region. The action curves of the nanorods accurately reproduce their extinction spectra, with a maximum IPCE of around 8.4% when they are immersed in an electron-donor solution. Strikingly, the photoelectric conversion

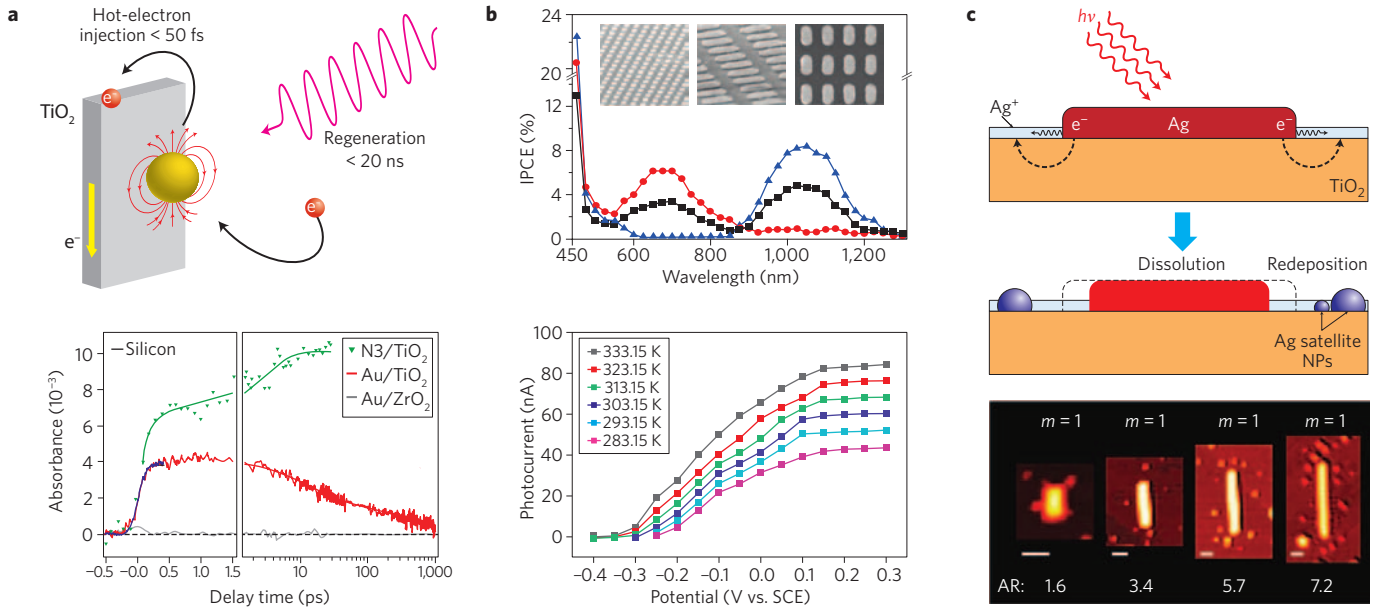

Figure 3 | Hot-electron regeneration and shape effects. a, Ultrafast visible-pump/infrared-probe femtosecond transient absorption spectroscopy shows the timescale of hot-electron injection in the TiO_2 conduction band[62]. **b**, SEM images for nanopatterned Au nanorods. The dimensions of the Au nanorods are 100 nm × 240 nm × 40 nm. The action spectra corresponding to non-polarized light (black), polarized light along the minor (red) and major (blue) axis directions of the nanorods reproduce the extinction spectra. Also, a progressive increase in the photocurrent is observed with increasing temperature[29]. **c**, Oxidation of Ag nanorods and redeposition of small Ag nanoparticles takes place as a result of plasmon-induced charge separation. After LSPR excitation and hot-electron generation, the oxidized Ag^+ ions diffuse in the water layer adsorbed on the TiO_2 substrate and eventually recombine with electrons from TiO_2, forming satellite redeposited islands. The atomic force microscopy images show Ag nanorods with various aspect ratios (ARs) that have undergone excitation of multipole plasmon modes from $m = 1$ to 4 after irradiation with 800 nm. The rods experience changes in length depending on the incident wavelength and mode excited. Horizontal scale bars are 50 nm (ref. 71). Figure reproduced with permission from: **a**, ref. 62, © 2007 ACS; **b**, ref. 29, © 2010 ACS; **c**, ref. 71, © 2012 ACS.

efficiency obtained with these plasmonic structures increases with increasing temperature, in contrast to the general trend of semiconductor-based solar cells (Fig. 3b, bottom). Plasmonic energy conversion could thus solve the overheating problem that afflicts conventional photovoltaic cells[69].

Several works have provided insights into the localization of hot-electron generation in plasmonic nanostructures. Kazuma *et al.*[70,71] showed that sites in Ag nanorods on TiO_2 exposed to higher electromagnetic fields generate more hot electrons. After LSPR excitation and hot-electron generation, the oxidized Ag^+ ions diffuse in the water layer adsorbed on the TiO_2 substrate, and eventually recombine with electrons from TiO_2, leading to the formation of satellite redeposited islands (Fig. 3c, top). This effect was observed in rods with different aspect ratios that sustained different multipole plasmon modes (m is 1–4), as shown in the atomic force microscopy images shown in the bottom portion of Fig. 3c. Islands appeared in locations where the LSPR electromagnetic field was more intense, confirming the hypothesis that the charge generation process is induced and/or promoted by the intense electromagnetic fields in the plasmonic nanostructures. Optimizing the design of plasmonic nanostructures so as to maximize the electromagnetic fields will increase hot-electron generation.

The geometry and the locations of the plasmonic nanostructures relative to the neighbouring semiconductor material are also very important. Knight *et al.*[12] showed that the photocurrent generated by an active plasmonic element can be significantly enhanced by embedding it in the neighbouring semiconductor, as this permits more efficient transfer of hot electrons. Also, as shown below, direct contact between the donor solution or HTM and the semiconductor material should be avoided to prevent detrimental carrier recombination.

Towards solid-state devices. Electron-donor solutions and HTMs play a key role in regenerating the carriers after hot-electron injection. Tian and Tatsuma[6] compared the performances of seven different donor solutions: $[Fe(CN)_6]^{4-}$, I^-, Fe^{2+}, ferrocenecarboxylic acid, Br^-, 1,1′-ferrocenedicarboxylic acid and Cl^-. They reported an IPCE of 12% at around 560 nm when Fe^{2+} was used as an electron donor. They obtained an extremely high IPCE of 26% on the addition of 4-nitrobenzoic acid, which they attributed to the acid being adsorbed on exposed TiO_2 and blocking the recombination of electrons. Subsequent studies[63,64] associated the higher efficiency of Fe^{2+} to faster carrier regeneration rates.

Carrier regeneration using liquid electrolytes is advantageous for photocatalysis applications as the liquid electrolyte facilitates the flow of the processing chemicals past the plasmonic nanostructures. In contrast, liquid cells are impractical for photovoltaic applications because of their lack of stability and problems with leaking and evaporation. In recent years, several solid-state plasmonic solar cell structures have been proposed, bringing practical application one step closer. Initial results for solid-state photovoltaic cells with organic and inorganic HTMs were unsatisfactory; the efficiencies obtained were very low, being around four orders of magnitude lower than those of liquid cells with an electrolyte containing a redox couple. Yu *et al.*[72] tested different solid-state cell architectures in which Au nanoparticles are in contact with TiO_2 and various HTMs, including poly(N-vinylcarbazole) (PVK), N,N′-bis(3-methylphenyl)-N,N′-diphenyl-[1,1′-biphenyl]-4,4′-diamine (TPD), CuI and CuSCN. They obtained a very low maximum IPCE of 0.0024% using PVK, which they attributed to carrier recombination caused by contact between the HTM and TiO_2. They also considered possible degradation of the HTM layers. Surprisingly, higher efficiencies were obtained in subsequent

studies that did not include any specific electrolyte or HTM layer. Takahashi and Tatsuma[73,74] showed that devices consisting of Au and Ag nanoparticles on TiO_2 and in contact with indium–tin oxide (ITO), where electrons are simply injected into the nanoparticles from the ITO film, can achieve IPCEs of around 0.4% and 0.6% for Au and Ag nanoparticles, respectively. Tian *et al.*[64] recently produced solid-state solar cells with considerably higher efficiencies (an IPCE as high as 6%) by using a similar architecture consisting of Au nanoparticles on TiO_2 and polyethylene oxide filled with TiO_2 nanoparticles as the HTM, which contains optimized redox couples I^-/I_3^-. Recently, Reineck *et al.*[75] used Spiro-OMeTAD as the HTM film in solid-state cells with self-assembled Au and Ag nanoparticles, obtaining IPCEs of 4.9 and 3.8%, respectively. Although recent advances in this field are encouraging, further research is needed to obtain HTMs and architectures that prevent carrier recombination occurring through direct contact with the semiconducting material.

Other applications and approaches. The injection of hot electrons from plasmonic nanoparticles into the semiconductor matrix on illumination significantly changes the conductivity of the system. Several studies have explored the possibility of using this principle to obtain plasmo-electronic devices in which the conductivity is controlled by varying the intensity of the visible light illumination. In recent studies[76,77], this effect has been observed in nanoparticles stabilized with different self-assembled monolayers, which increased or reduced the electrical conductivity of the material during resonance, depending on whether they contained neutral or charged ligands, respectively. Mubeen *et al.*[78] proposed devices consisting of Au nanoparticles and TiO_2 multilayers in which hot-electron tunnelling produced an over 1,000-fold increase in the conductance on illumination by 600 nm light. Son *et al.*[79] reported surface-plasmon-enhanced photoconductance in TiO_2 nanofibres loaded with Au nanoparticles. Several other works have focused on plasmonic photoinduced currents in nanodiode structures. Lee *et al.*[80] observed an enhanced photocurrent as a result of plasmon-assisted generation of hot electrons on nanodiodes consisting of gold islands on TiO_2; the photocurrent can be further enhanced by incorporating dye molecules[81]. Knight *et al.*[7] observed hot-electron flows induced by infrared irradiation of Au/Si nanoantennas. Wadell *et al.*[82] investigated Au–SiO_2–Pd nanoantennas. Also, manipulation of plasmonic resonance by changing the electronic density has been proposed for applications such as smart windows and displays[83].

So far, only a few works have explored plasmonic charge separation using propagating surface plasmon polaritons (SPPs). The use of SPPs is interesting as they cannot decay directly into photons unless surface roughness is present[24]; thus, non-radiative decay is the only mechanism possible in flat films. Wang *et al.*[8] proposed a new architecture based on SPP excitation in a metal–insulator–metal structure illuminated under the prism coupler configuration. Owing to the high localization of SPPs on the top metal thin film, more hot electrons are transmitted from the top electrode to the bottom electrode than in the opposite direction, leading to the detection of a net photocurrent. Wang *et al.*'s calculations suggest that this kind of architecture could achieve efficiencies of up to 4.3% for 640-nm irradiation of Ag films, and of up to 3.5% for 780-nm irradiation of Au films. Nevertheless, in practice, they were only able to measure efficiencies of around 2.7%, as a result of surface recombination at the metal–insulator interface. Along the same lines, Pradhan *et al.*[84] investigated semiconductor–insulator–semiconductor heterojunctions consisting of Al:ZnO/SiO_2/Si.

New directions in plasmonic energy conversion

Plasmonic hot-electron generation is a very promising energy conversion process. However, it requires new advances in order to approach the record efficiencies achieved by state-of-the-art semiconductor solar cells. Several aspects directly related to the nature of these devices need to be considered, including the materials used to fabricate the plasmonic nanostructures, the semiconductors used to capture the photoexcited hot electrons, their architectures and even the fabrication method. This section reviews and discusses some of the most important aspects that need major advances to further improve the efficiency of this energy conversion method.

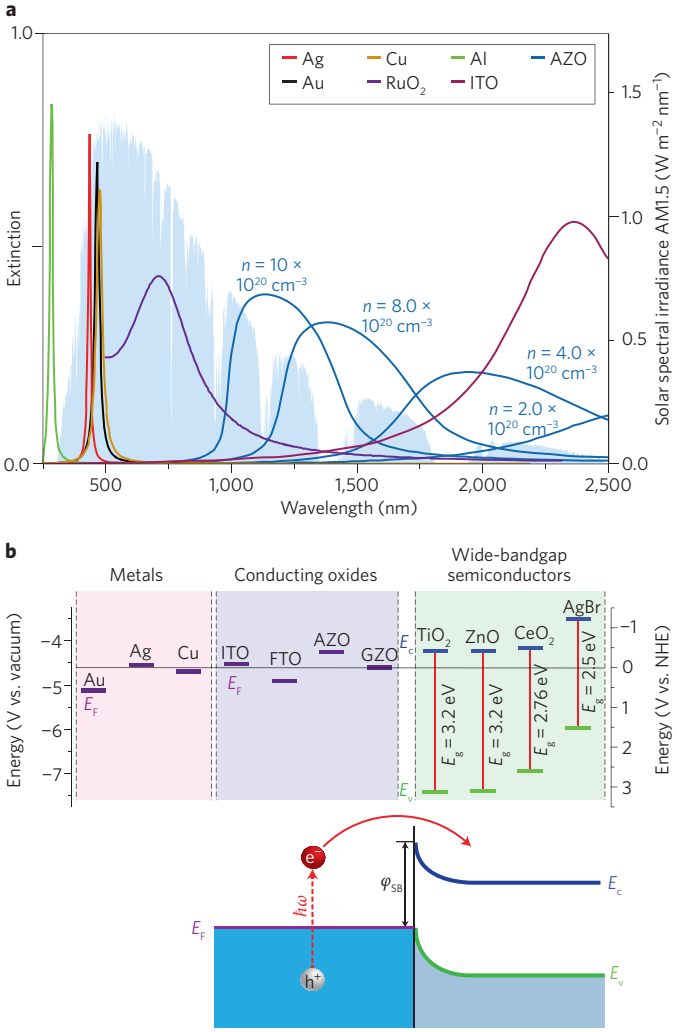

Figure 4 | Materials for plasmonic solar cells. a, Optical extinction of metal (Al, Ag, Au and Cu) and conducting oxides (RuO_2, AZO and ITO) plasmonic nanostructures. The solar irradiance spectrum is plotted in the background. **b**, Fermi level (E_F), conduction (E_c) and valence (E_v) bands energy for selected metals, conducting oxides and wide-bandgap semiconductors of interest for the fabrication of plasmonic nanostructures. The energies are plotted on a potential scale (V) versus the normal hydrogen electrode (NHE) and also versus vacuum. The values for E_c and E_v for TiO_2, ZnO, CeO_2 and AgBr were obtained from refs 19, 9, 100 and 101, respectively. The E_F values for Au, Ag, Cu, ITO, FTO, AZO and GZO were obtained from refs 64, 4, 93 and 102–105, respectively.

Efficiency and fabrication cost of plasmonic versus conventional photovoltaic devices. A very important point that needs to be carefully considered is the efficiency of the plasmonic devices relative to that of conventional photovoltaic cells. Currently, the most commonly used solar cells are based on crystalline Si (c-Si).

Commercial solar cells generally have average efficiencies in the range 16–20%, although efficiencies has high as 28.3% have recently been achieved in single-junction solar cells[85]. Second-generation photovoltaic devices consisting of thin-film cells made from amorphous silicon, CdTe or copper–indium–gallium diselenide (CIGS) deposited on cheap substrates such as plastic, glass or stainless steel have achieved efficiencies of up to 20.3% (ref. 85). Third-generation devices encompass a large range of new technologies, including multijunction cells, multiband cells, hot-carrier cells and solar thermal technologies[86]. Because they employ several semiconductors with different bandgaps, multijunction solar cells have considerably broader absorption spectra than single-junction solar cells. This approach recently resulted in a record efficiency of 43.5% being realized under concentrated illumination[85]. In contrast, the maximum efficiency achieved to date in dye-sensitized solar cells based on hot-electron generation is only 11.4% (ref. 85). In contrast, plasmonic solar cells based on hot-electron generation are still in their infancy; their efficiencies are discussed below.

The energy from surface plasmon decay is transferred to electrons over the whole DOS distribution of the nanostructure's conduction band. This creates a very broad distribution of hot-electron states above the Fermi energy, so that many hot electrons may have insufficient energy to be injected into the semiconductor. White and Catchpole[25] estimated the efficiency limit of Schottky-barrier-based plasmonic energy conversion devices. Assuming a parabolic DOS for the conduction band of metals such as Ag and Au, a Schottky barrier energy of φ_{SB} = 1.2 eV, and an equal photoexcitation probability for all the electrons in the conduction band, results in a maximum IPCE of 8%. However, photoemission experiments in noble metals indicate that electrons close to the Fermi energy are preferentially excited over lower energy electrons[26], which considerably increases the efficiency of this process. To reflect this observation, White and Catchpole[25] also performed calculations for a more realistic model in which the effective conduction band edge is 0.15 eV below the Fermi level. Such a narrow DOS distribution makes the emission efficiency approach a step-like function in which the probability of hot electrons with energies higher than φ_{SB} crossing the barrier approaches 100%. For this case, they calculated a considerably higher efficiency of 22.6% for φ_{SB} = 1.4 eV. Further engineering of the DOS of the plasmonic material to favour preferential excitation of electronic levels close to the Fermi energy, such as in semiconductor-based plasmonic nanostructures, along with tuning of the Schottky barrier, will allow efficiencies well in excess of 22% (ref. 25). Furthermore, the use of materials with LSPR frequencies spread over the whole solar spectrum will enable more efficient utilization of the solar radiation, as shown in the next subsection.

Efficiencies higher than 22% certainly make plasmonic solar cells an interesting alternative. However, the success of this technology is dependent on realizing a high efficiency while keeping fabrication costs low. The cost of Si has dropped over the past few years, but c-Si solar cells require relatively thick (180–300 μm) films with their associated expensive processing[87]. Second- and third-generation thin-film-based solar cells are cheaper to fabricate, but their materials have poor light trapping, so that plasmonic and dielectric light-trapping mechanisms are required[3]. In this sense, plasmonic solar cells combine the low fabrication costs of second-generation solar cells with the highly efficient light trapping of their plasmonic elements.

The method used for fabricating plasmonic energy conversion devices also greatly affects their cost. So far, they have been mostly fabricated by inexpensive solution-based methods in which commercially available noble metal and semiconductor nanoparticles are properly combined[5,34,65,72]. Noble metal nanoparticles of controlled size have also been obtained by photocatalysis[6,37,63,70], electrodeposition[35,74], electrodeposition through a thin alumina nanomask[73], electrostatic self-assembly[75] and by a modified Turkevich method[33,88]. More complicated structures, such as core–shell nanoparticles, have been fabricated[60,61]. Also, noble metal nanoparticle-decorated TiO_2 nanotubes have been fabricated by the hydrothermal method[45] and electrochemical anodic oxidation[48,49]. Only a few studies have used lithography to achieve more elaborate plasmonic nanostructure shapes, such as nanorods[10,29] and nanowires[12]. Although the above-mentioned techniques are useful for demonstrating this energy conversion method, scalable techniques that provide a high degree of homogeneity over larger areas together with fine control of the sizes and shapes of nanostructures will be needed to further develop and eventually commercialize these kinds of devices. To realize these goals, techniques based on physical vapour deposition that have been modified to enable nanoparticles to be created from a high-pressure plasma are promising[89–91]. They allow reactive gases such as oxygen to be added, enabling the formation of size-controlled nanoparticles of oxides such as TiO_2, aluminium-doped zinc oxide (AZO) and ITO. Other emerging technologies, such as nanoimprinting, should also be considered for this application[92]. The use of such techniques will lead to important breakthroughs in the development of this technology.

Plasmonic materials and semiconductor acceptors for optimized solar absorption. So far, noble metals such as Ag and Au have been virtually the only materials used in plasmonic energy conversion. Noble-metal nanostructures exhibit very intense LSPR excitations, which give rise to very strong light absorption, mainly in the visible region. The frequency at which plasmonic nanostructures undergo LSPR strongly depends on their carrier concentration. For spherical nanoparticles in air, LSPR occurs at a frequency of $\omega_{LSPR} \approx \omega_p/\sqrt{3}$, where the plasma frequency ω_p directly depends on the carrier concentration n_e according to[67]

$$\omega_p = \sqrt{\frac{n_e e^2}{m^* \varepsilon_0}} \quad (1)$$

where e is the charge of an electron, m^* is the effective mass of an electron and ε_0 is the permittivity of free space. Figure 4a shows the calculated optical extinction (that is, optical absorption) for Al, Ag, Au and Cu nanoparticles superimposed on the solar spectral irradiance AM1.5. These nanoparticles have very intense but narrow absorptions in the lower wavelength region of the visible range because of their relatively high carrier concentrations[93] (around 5.9×10^{22} cm^{-3} for Ag and Au). However, a significant portion of the solar radiation that reaches the Earth's surface has longer wavelengths; about 40% of the solar radiation has a wavelength longer than 800 nm (ref. 29). It is therefore of paramount importance to find materials that allow us to use a greater portion of the solar spectrum. Conducting oxides and semiconductors have lower carrier concentrations than noble metals, and hence lower plasma frequencies, placing their resonances in the near-infrared range. Figure 4a shows the calculated extinctions of the widely used conducting oxides RuO_2, aluminium-doped zinc oxide (AZO) and ITO. Conducting oxides have broader absorptions than noble metals, mainly because of their higher optical losses[94]. The use of plasmonic nanostructures made from conducting oxides to capture and convert the infrared region of the solar spectrum will extend the range of application of plasmonic solar cells, significantly increasing their overall efficiency.

Furthermore, it is possible to use the doping concentration in conducting oxides such as AZO and ITO to tune their carrier

concentration, and hence the spectral region in which plasmonic resonance takes place. For example, the carrier concentration of AZO can be varied in the range $0.5–10 \times 10^{20}$ cm^{-3} by changing the concentration of Al; this enables the surface plasmon resonance to be varied over the wide range of 2,200–880 nm (ref. 95), as shown in Fig. 4a. In addition, it is possible to create alloys of two or more metals with fine-tuned plasmonic properties[96]. Nanostructures made from noble-metal–transition-metal alloys are the best candidates for this application because their Fermi level and surface plasma frequency ω_{LSPR} can be modified. Other materials, such as conducting transition-metal nitrides (for example, TiN, ZrN, HfN and TaN) are interesting for plasmonic applications as they exhibit metallic properties at visible frequencies[97,98]. Analogous to multiple-junction solar cells in which semiconductors with different bandgaps are combined in order to cover the whole solar spectrum, systems that combine multiple metals and conducting oxides will permit the absorption spectrum of the devices to be matched to the solar spectrum.

The semiconductor used to trap the photoexcited hot electrons greatly affects the charge injection mechanism. Important factors to consider are the bandgap of the semiconductor, which affects the height of the semiconductor–metal Schottky barrier, and the density of available states in the conduction band, which affects the efficiency of the hot-electron injection process. Good alignment of the Fermi level of the plasmonic nanostructures with the bands of the semiconductor is important to favour efficient carrier injection[99]. As shown in Fig. 4b, the Fermi energy level is around 0 V on the normal hydrogen electrode scale[9] for noble metals and conducting oxides. The energy at which surface plasmons transfer to hot electrons on decay has been shown to depend strongly on the material, and the size and shape of the plasmonic nanostructures; it typically ranges between 1 eV and 4 eV for Au and Ag nanostructures[9,20,27]. Thus, the semiconductor needs to be chosen such that the photoexcited hot electrons can overcome the Schottky barrier φ_{SB}. Figure 4b depicts the positions of the conduction and valence bands of several wide-bandgap semiconductors of interest for plasmonic energy conversion. TiO_2 is by far the most frequently used semiconductor material. It has a wide bandgap (E_g = 3.3 eV) and an excellent electron-accepting ability because of the high DOS in its conduction band. This is mainly because of the *d*-orbital nature of its conduction band; this contrasts with other typical metal oxides (such as ZnO, SnO_2 and In_2O_3) whose conduction bands are mainly composed of the *s* or *sp* orbital of the metal atoms[11]. These characteristics make TiO_2 an excellent candidate for this application. Nevertheless, other semiconductors such as ZnO, CeO_2 and AgBr have suitably positioned conduction and valence bands, and they can also serve as efficient electron acceptors. Further comparative studies are needed to determine the most suitable material based on the particular characteristics of the plasmonic nanostructures used.

Conclusions and outlook

Generation of hot electrons in plasmonic nanostructures is a very promising energy conversion mechanism, and it has found interesting applications in photovoltaic and photocatalytic devices. This review has covered the fundamentals of hot-electron generation, injection and regeneration in plasmonic nanostructures. Although still in its infancy, this field has witnessed considerable progress, offering potentially high energy conversion efficiencies while keeping fabrication costs low. Realizing fast hot-electron injection before recombination and optimal carrier regeneration are key factors that will allow higher conversion efficiencies to be obtained. In addition, the use of new plasmonic materials such as semiconductors and conducting oxides is proposed to extend the spectral range of light absorption and hot-electron generation, allowing optimum utilization of the solar spectrum.

Received 9 May 2013; accepted 2 August 2013; published 30 January 2014

References

1. Atwater, H. A. The promise of plasmonics. *Sci. Am.* **296,** 56–62 (2007).
2. Mendes, M. J., Luque, A., Tobías, I. & Martí, A. Plasmonic light enhancement in the near-field of metallic nanospheroids for application in intermediate band solar cells. *Appl. Phys. Lett.* **95,** 071105 (2009).
3. Atwater, H. A. & Polman, A. Plasmonics for improved photovoltaic devices. *Nature Mater.* **9,** 205–213 (2010).
4. Zhao, G., Kozuka, H. & Yoko, T. Sol—gel preparation and photoelectrochemical properties of TiO_2 films containing Au and Ag metal particles. *Thin Solid Films* **277,** 147–154 (1996).
5. Tian, Y. & Tatsuma, T. Plasmon-induced photoelectrochemistry at metal nanoparticles supported on nanoporous TiO_2. *Chem. Commun.* 1810–1811 (2004).
6. Tian, Y. & Tatsuma, T. Mechanisms and applications of plasmon-induced charge separation at TiO_2 films loaded with gold nanoparticles. *J. Am. Chem. Soc.* **127,** 7632–7637 (2005).
7. Knight, M. W., Sobhani, H., Nordlander, P. & Halas, N. J. Photodetection with active optical antennas. *Science* **332,** 702–704 (2011).
8. Wang, F. & Melosh, N. A. Plasmonic energy collection through hot carrier extraction. *Nano Lett.* **11,** 5426–5430 (2011).
9. Linic, S., Christopher, P. & Ingram, D. B. Plasmonic-metal nanostructures for efficient conversion of solar to chemical energy. *Nature Mater.* **10,** 911–921 (2011).
10. Nishijima, Y. *et al.* Near-infrared plasmon-assisted water oxidation. *J. Phys. Chem. Lett.* **3,** 1248–1252 (2012).
11. Du, L., Furube, A., Hara, K., Katoh, R. & Tachiya, M. Ultrafast plasmon induced electron injection mechanism in gold–TiO_2 nanoparticle system. *J. Photochem. Photobiol. C* **15,** 21–30 (2013).
12. Knight, M. W. *et al.* Embedding plasmonic nanostructure diodes enhances hot electron emission. *Nano Lett.* **13,** 1687–1692 (2013).
13. Mubeen, S. *et al.* An autonomous photosynthetic device in which all charge carriers derive from surface plasmons. *Nature Nanotechnol.* **8,** 247–251 (2013).
14. Semenov, A. D., Gol'tsman, G. N. & Sobolewski, R. Hot-electron effect in superconductors and its applications for radiation sensors. *Supercond. Sci. Technol.* **15,** R1 (2002).
15. Hertz, H. Ueber einen Einfluss des ultravioletten Lichtes auf die electrische Entladung. *Ann. Phys.* **267,** 983–1000 (1887).
16. Gadzuk, J. W. On the detection of chemically-induced hot electrons in surface processes: from X-ray edges to Schottky barriers. *J. Phys. Chem. B* **106,** 8265–8270 (2002).
17. Nienhaus, H. Electronic excitations by chemical reactions on metal surfaces. *Surf. Sci. Rep.* **45,** 1–78 (2002).
18. O'Regan, B. & Grätzel, M. A low-cost, high-efficiency solar cell based on dye-sensitized colloidal TiO_2 films. *Nature* **353,** 737–740 (1991).
19. Grätzel, M. Photoelectrochemical cells. *Nature* **414,** 338–344 (2001).
20. Sönnichsen, C. *et al.* Drastic reduction of plasmon damping in gold nanorods. *Phys. Rev. Lett.* **88,** 077402 (2002).
21. Hofmann, J. & Steinmann, W. Plasma resonance in the photoemission of silver. *Phys. Status Solidi B* 30, K53–K56 (1968).
22. Endriz, J. G. & Spicer, W. E. Surface-plasmon-one-electron decay and its observation in photoemission. *Phys. Rev. Lett.* **24,** 64–68 (1970).
23. Lehmann, J. *et al.* Surface plasmon dynamics in silver nanoparticles studied by femtosecond time-resolved photoemission. *Phys. Rev. Lett.* **85,** 2921–2924 (2000).
24. Inagaki, T., Kagami, K. & Arakawa, E. T. Photoacoustic observation of nonradiative decay of surface plasmons in silver. *Phys. Rev. B* **24,** 3644–3646 (1981).
25. White, T. P. & Catchpole, K. R. Plasmon-enhanced internal photoemission for photovoltaics: theoretical efficiency limits. *Appl. Phys. Lett.* **101,** 073905 (2012).
26. Berglund, C. N. & Spicer, W. E. Photoemission studies of copper and silver: experiment. *Phys. Rev.* **136,** A1044–A1064 (1964).
27. Rycenga, M. *et al.* Controlling the synthesis and assembly of silver nanostructures for plasmonic applications. *Chem. Rev.* **111,** 3669–3712 (2011).
28. Moskovits, M. Hot electrons cross boundaries. *Science* **332,** 676–677 (2011).
29. Nishijima, Y., Ueno, K., Yokota, Y., Murakoshi, K. & Misawa, H. Plasmon-assisted photocurrent generation from visible to near-infrared wavelength using a Au-nanorods/TiO_2 electrode. *J. Phys. Chem. Lett.* **1,** 2031–2036 (2010).
30. Ohko, Y. *et al.* Multicolour photochromism of TiO_2 films loaded with silver nanoparticles. *Nature Mater.* **2,** 29–31 (2003).
31. Naoi, K., Ohko, Y. & Tatsuma, T. TiO_2 films loaded with silver nanoparticles: control of multicolor photochromic behavior. *J. Am. Chem. Soc.* **126,** 3664–3668 (2004).
32. Hirakawa, T. & Kamat, P. V. Photoinduced electron storage and surface plasmon modulation in Ag@TiO_2 clusters. *Langmuir* **20,** 5645–5647 (2004).

33. Lana-Villarreal, T. & Gómez, R. Tuning the photoelectrochemistry of nanoporous anatase electrodes by modification with gold nanoparticles: development of cathodic photocurrents. *Chem. Phys. Lett.* **414,** 489–494 (2005).
34. Yu, K., Tian, Y. & Tatsuma, T. Size effects of gold nanaoparticles on plasmon-induced photocurrents of gold–TiO_2 nanocomposites. *Phys. Chem. Chem. Phys.* **8,** 5417–5420 (2006).
35. Sakai, N., Fujiwara, Y., Takahashi, Y. & Tatsuma, T. Plasmon-resonance-based generation of cathodic photocurrent at electrodeposited gold nanoparticles coated with TiO_2 films. *ChemPhysChem* **10,** 766–769 (2009).
36. Kowalska, E., Abe, R. & Ohtani, B. Visible light-induced photocatalytic reaction of gold-modified titanium(IV) oxide particles: action spectrum analysis. *Chem. Commun.* 241–243 (2009).
37. Toyoda, T., Tsugawa, S. & Shen, Q. Photoacoustic spectra of Au quantum dots adsorbed on nanostructured TiO_2 electrodes together with the photoelectrochemical current characteristics. *J. Appl. Phys.* **105,** 034314 (2009).
38. Gomes Silva, C., Juárez, R., Marino, T., Molinari, R. & García, H. Influence of excitation wavelength (UV or visible light) on the photocatalytic activity of titania containing gold nanoparticles for the generation of hydrogen or oxygen from water. *J. Am. Chem. Soc.* **133,** 595–602 (2010).
39. Kowalska, E., Mahaney, O. O. P., Abe, R. & Ohtani, B. Visible-light-induced photocatalysis through surface plasmon excitation of gold on titania surfaces. *Phys. Chem. Chem. Phys.* **12,** 2344–2355 (2010).
40. Ide, Y., Matsuoka, M. & Ogawa, M. Efficient visible-light-induced photocatalytic activity on gold-nanoparticle-supported layered titanate. *J. Am. Chem. Soc.* **132,** 16762–16764 (2010).
41. Valverde-Aguilar, G., García-Macedo, J. A., Rentería-Tapia, V. & Aguilar-Franco, M. Photoconductivity studies on amorphous and crystalline TiO_2 films doped with gold nanoparticles. *Appl. Phys. A* **103,** 659–663 (2011).
42. Ingram, D. B., Christopher, P., Bauer, J. L. & Linic, S. Predictive model for the design of plasmonic metal/semiconductor composite photocatalysts. *ACS Catal.* **1,** 1441–1447 (2011).
43. Tanaka, A. *et al.* Gold–titanium(IV) oxide plasmonic photocatalysts prepared by a colloid-photodeposition method: correlation between physical properties and photocatalytic activities. *Langmuir* **28,** 13105–13111 (2012).
44. Shi, X., Ueno, K., Takabayashi, N. & Misawa, H. Plasmon-enhanced photocurrent generation and water oxidation with a gold nanoisland-loaded titanium dioxide photoelectrode. *J. Phys. Chem. C* **117,** 2494–2499 (2013).
45. Gong, D. *et al.* Silver decorated titanate/titania nanostructures for efficient solar driven photocatalysis. *J. Solid State Chem.* **189,** 117–122 (2012).
46. Sakai, N., Sasaki, T., Matsubara, K. & Tatsuma, T. Layer-by-layer assembly of gold nanoparticles with titania nanosheets: control of plasmon resonance and photovoltaic properties. *J. Mater. Chem.* **20,** 4371–4378 (2010).
47. Shiraishi, Y. *et al.* Platinum nanoparticles supported on anatase titanium dioxide as highly active catalysts for aerobic oxidation under visible light irradiation. *ACS Catal.* **2,** 1984–1992 (2012).
48. Wu, F. *et al.* Photocatalytic activity of Ag/TiO_2 nanotube arrays enhanced by surface plasmon resonance and application in hydrogen evolution by water splitting. *Plasmonics* **8,** 501–508 (2012).
49. Chen, K. *et al.* Effect of Ag nanoparticle size on the photoelectrochemical properties of Ag decorated TiO_2 nanotube arrays. *J. Alloys Compd* **554,** 72–79 (2013).
50. Chen, Z. H. *et al.* Vertically aligned ZnO nanorod arrays sentisized with gold nanoparticles for Schottky barrier photovoltaic cells. *J. Phys. Chem. C* **113,** 13433–13437 (2009).
51. Chen, H. M. *et al.* Plasmon inducing effects for enhanced photoelectrochemical water splitting: X-ray absorption approach to electronic structures. *ACS Nano* **6,** 7362–7372 (2012).
52. Han, Z. *et al.* Visible-light photocatalytic application of hierarchical Au-ZnO flower-rod heterostructures via surface plasmon resonance. *Plasmonics* **8,** 1193–1202 (2013).
53. Primo, A., Marino, T., Corma, A., Molinari, R. & García, H. Efficient visible-light photocatalytic water splitting by minute amounts of gold supported on nanoparticulate CeO_2 obtained by a biopolymer templating method. *J. Am. Chem. Soc.* **133,** 6930–6933 (2011).
54. Kominami, H., Tanaka, A. & Hashimoto, K. Mineralization of organic acids in aqueous suspensions of gold nanoparticles supported on cerium(IV) oxide powder under visible light irradiation. *Chem. Commun.* **46,** 1287–1289 (2010).
55. Chen, X., Li, P., Tong, H., Kako, T. & Ye, J. Nanoarchitectonics of a Au nanoprism array on WO_3 film for synergistic optoelectronic response. *Sci. Technol. Adv. Mater.* **12,** 044604 (2011).
56. Zhou, X., Hu, C., Hu, X., Peng, T. & Qu, J. Plasmon-assisted degradation of toxic pollutants with Ag–AgBr/Al_2O_3 under visible-light irradiation. *J. Phys. Chem. C* **114,** 2746–2750 (2010).
57. Hu, C. *et al.* Plasmon-induced photodegradation of toxic pollutants with Ag–AgI/Al_2O_3 under visible-light irradiation. *J. Am. Chem. Soc.* **132,** 857–862 (2009).
58. Wang, P. *et al.* Ag@AgCl: a highly efficient and stable photocatalyst active under visible light. *Angew. Chem.* **47,** 7931–7933 (2008).
59. Kochuveedu, S. T., Kim, D.-P. & Kim, D. H. Surface-plasmon-induced visible light photocatalytic activity of TiO_2 nanospheres decorated by Au nanoparticles with controlled configuration. *J. Phys. Chem. C* **116,** 2500–2506 (2012).
60. Zhang, N., Liu, S., Fu, X. & Xu, Y.-J. Synthesis of M@TiO_2 (M = Au, Pd, Pt) core-shell nanocomposites with tunable photoreactivity. *J. Phys. Chem. C* **115,** 9136–9145 (2011).
61. Zheng, Z. *et al.* Facile *in situ* synthesis of visible-light plasmonic photocatalysts M@TiO_2 (M = Au, Pt, Ag) and evaluation of their photocatalytic oxidation of benzene to phenol. *J. Mater. Chem.* **21,** 9079–9087 (2011).
62. Furube, A., Du, L., Hara, K., Katoh, R. & Tachiya, M. Ultrafast plasmon-induced electron transfer from gold nanodots into TiO_2 nanoparticles. *J. Am. Chem. Soc.* **129,** 14852–14853 (2007).
63. Tian, Y., Wang, X., Zhang, D., Shi, X. & Wang, S. Effects of electron donors on the performance of plasmon-induced photovoltaic cell. *J. Photochem. Photobiol., A* **199,** 224–229 (2008).
64. Tian, Y., Shi, X., Lu, C., Wang, X. & Wang, S. Charge separation in solid-state gold nanoparticles-sensitized photovoltaic cell. *Electrochem. Commun.* **11,** 1603–1605 (2009).
65. Du, L. *et al.* Plasmon-induced charge separation and recombination dynamics in gold–TiO_2 nanoparticle systems: dependence on TiO_2 particle size. *J. Phys. Chem. C* **113,** 6454–6462 (2009).
66. Inouye, H., Tanaka, K., Tanahashi, I. & Hirao, K. Ultrafast dynamics of nonequilibrium electrons in a gold nanoparticle system. *Phys. Rev. B* **57,** 11334–11340 (1998).
67. Kreibig, U. & Vollmer, M. *Optical Properties of Metal Clusters*. (Springer, 1995).
68. Langhammer, C., Yuan, Z., Zorić, I. & Kasemo, B. Plasmonic properties of supported Pt and Pd nanostructures. *Nano Lett.* **6,** 833–838 (2006).
69. Skoplaki, E. & Palyvos, J. A. On the temperature dependence of photovoltaic module electrical performance: a review of efficiency/power correlations. *Sol. Energy* **83,** 614–624 (2009).
70. Kazuma, E., Sakai, N. & Tatsuma, T. Nanoimaging of localized plasmon-induced charge separation. *Chem. Commun.* **47,** 5777–5779 (2011).
71. Kazuma, E. & Tatsuma, T. Photoelectrochemical analysis of allowed and forbidden multipole plasmon modes of polydisperse Ag nanorods. *J. Phys. Chem. C* **117,** 2435–3441 (2013).
72. Yu, K., Sakai, N. & Tatsuma, T. Plasmon resonance-based solid-state photovoltaic devices. *Electrochem. Commun.* **76,** 161 (2008).
73. Takahashi, Y. & Tatsuma, T. Electrodeposition of thermally stable gold and silver nanoparticle ensembles through a thin alumina nanomask. *Nanoscale* **2,** 1494–1499 (2010).
74. Takahashi, Y. & Tatsuma, T. Solid state photovoltaic cells based on localized surface plasmon-induced charge separation. *Appl. Phys. Lett.* **99,** 182110–182113 (2011).
75. Reineck, P. *et al.* A solid-state plasmonic solar cell via metal nanoparticle self-assembly. *Adv. Mater.* **24,** 4750–4755 (2012).
76. Nakanishi, H. *et al.* Photoconductance and inverse photoconductance in films of functionalized metal nanoparticles. *Nature* **460,** 371–375 (2009).
77. Warren, S. C., Walker, D. A. & Grzybowski, B. A. Plasmoelectronics: coupling plasmonic excitation with electron flow. *Langmuir* **28,** 9093–9102 (2012).
78. Mubeen, S., Hernandez-Sosa, G., Moses, D., Lee, J. & Moskovits, M. Plasmonic photosensitization of a wide band gap semiconductor: converting plasmons to charge carriers. *Nano Lett.* **11,** 5548–5552 (2011).
79. Son, M.-S. *et al.* Surface plasmon enhanced photoconductance and single electron effects in mesoporous titania nanofibers loaded with gold nanoparticles. *Appl. Phys. Lett.* **96,** 023115 (2010).
80. Lee, Y. K. *et al.* Surface plasmon-driven hot electron flow probed with metal-semiconductor nanodiodes. *Nano Lett.* **11,** 4251–4255 (2011).
81. Lee, Y. K., Park, J. & Park, J. Y. The effect of dye molecules and surface plasmons in photon-induced hot electron flows detected on Au/TiO_2 nanodiodes. *J. Phys. Chem. C* **116,** 18591–18596 (2012).
82. Wadell, C., Antosiewicz, T. J. & Langhammer, C. Optical absorption engineering in stacked plasmonic Au-SiO_2-Pd nanoantennas. *Nano Lett.* **12,** 4784–4790 (2012).
83. Garcia, G. *et al.* Dynamically modulating the surface plasmon resonance of doped semiconductor nanocrystals. *Nano Lett.* **11,** 4415–4420 (2011).
84. Pradhan, A. K., Holloway, T., Mundle, R., Dondapati, H. & Bahoura, M. Energy harvesting in semiconductor-insulator-semiconductor junctions through excitation of surface plasmon polaritons. *Appl. Phys. Lett.* **100,** 061127 (2012).
85. Green, M. A., Emery, K., Hishikawa, Y., Warta, W. & Dunlop, E. D. Solar cell efficiency tables (version 39). *Prog. Photovoltaics Res. Appl.* **20,** 12–20 (2012).

86. Green, M. A. Third generation photovoltaics: solar cells for 2020 and beyond. *Physica E* **14,** 65–70 (2002).
87. Mokkapati, S. & Catchpole, K. R. Nanophotonic light trapping in solar cells. *J. Appl. Phys.* **112,** 101101 (2012).
88. Atar, F. B. *et al.* Plasmonically enhanced hot electron based photovoltaic device. *Opt. Express* **21,** 7196–7201 (2013).
89. Binns, C. Nanoclusters deposited on surfaces. *Surf. Sci. Rep.* **44,** 1–49 (2001).
90. Palmer, R. E., Pratontep, S. & Boyen, H.-G. Nanostructured surfaces from size-selected clusters. *Nature Mater.* **2,** 443–448 (2003).
91. Wegner, K., Piseri, P., Vahedi-Tafreshi, H. & Milani, P. Cluster beam deposition: a tool for nanoscale science and technology. *J. Phys. D* **39,** R439 (2006).
92. Perelaer, J. & Schubert, U. S. Novel approaches for low temperature sintering of inkjet-printed inorganic nanoparticles for roll-to-roll (R2R) applications. *J. Mater. Res.* **28,** 564–573 (2013).
93. Kittel, C. *Introduction to Solid State Physics*. (Wiley, 1976).
94. Hövel, H., Fritz, S., Hilger, A., Kreibig, U. & Vollmer, M. Width of cluster plasmon resonances: bulk dielectric functions and chemical interface damping. *Phys. Rev. B* **48,** 18178–18188 (1993).
95. Mendelsberg, R. J. *et al.* Achieving high mobility ZnO:Al at very high growth rates by dc filtered cathodic arc deposition. *J. Phys. D* **44,** 232003 (2011).
96. West, P. R. *et al.* Searching for better plasmonic materials. *Las. Photon. Rev.* **4,** 795–808 (2010).
97. Naik, G. V., Kim, J. & Boltasseva, A. Oxides and nitrides as alternative plasmonic materials in the optical range. *Opt. Mater. Express* **1,** 1090–1099 (2011).
98. Naik, G. V. *et al.* Titanium nitride as a plasmonic material for visible and near-infrared wavelengths. *Opt. Mater. Express* **2,** 478–489 (2012).
99. Cushing, S. K. *et al.* Photocatalytic activity enhanced by plasmonic resonant energy transfer from metal to semiconductor. *J. Am. Chem. Soc.* **134,** 15033–15041 (2012).
100. Magesh, G., Viswanathan, B., Viswanath, R. P. & Varadarajan, T. K. Photocatalytic behavior of CeO_2-TiO_2 system for the degradation of methylene blue. *Indian J. Chem. A* **48,** 480–488 (2009).
101. Taft, E. A., Philipp, H. R. & Apker, L. Photoelectric emission from the valence band in AgBr. *Phys. Rev.* **110,** 876–878 (1958).
102. Park, Y., Choong, V., Gao, Y., Hsieh, B. R. & Tang, C. W. Work function of indium tin oxide transparent conductor measured by photoelectron spectroscopy. *Appl. Phys. Lett.* **68,** 2699–2701 (1996).
103. Helander, M. G., Greiner, M. T., Wang, Z. B., Tang, W. M. & Lu, Z. H. Work function of fluorine doped tin oxide. *J. Vac. Sci. Technol. A* **29,** 011019 (2011).
104. Wang, W. *et al.* Dependence of aluminum-doped zinc oxide work function on surface cleaning method as studied by ultraviolet and X-ray photoelectron spectroscopies. *Appl. Surf. Sci.* **257,** 3884–3887 (2011).
105. Yoshida, K., Aoki, T., Suzuki, A., Matsushita, T. & Okuda, M. Work function controlled transparent conductive films with zinc oxide system by pulsed laser deposition method. *J. Vac. Soc. Japan* **51,** 172–174 (2008).

Acknowledgements

The author thanks A. Anders and R. Mendelsberg for insightful discussions. This work was supported by the Assistant Secretary for Energy Efficiency and Renewable Energy, Office of Building Technology, of the US Department of Energy under Contract No. DE-AC02-05CH11231.

Additional information

Reprints and permissions information is available at www.nature.com/reprints. Correspondence and requests for materials should be addressed to the author.

Competing financial interests

The author declares no competing financial interests.